J. Astrophys. Astr. (2013) **34,** 357–372

Distribution of Doppler Redshifts of Associated Absorbers of SDSS Quasars

Cai-Juan Pan & Zhi-Fu Chen*

Department of Physics and Telecommunication Engineering of Baise University, Baise 533000, China

**e-mail: zhichenfu@126.com*

Received 13 May 2013; accepted 17 October 2013

Abstract. Doppler redshifts of a sample of Mg II associated absorbers of SDSS DR7 quasars are analysed. We find that there might be three Gaussian components in the distribution of the Doppler redshift. The first Gaussian component, with the peak being located at $z_{\rm Dopp} = -0.0074$, probably arises from absorbers with outflow histories observed in the direction close to jets of quasars. The second Gaussian component, with the peak being located at $z_{\rm Dopp} = -0.0017$, possibly arises from absorbers with outflow histories observed in the direction far away from jets of quasars. Whereas, the third Gaussian component, with the peak being located at $z_{\rm Dopp} = -0.0004$, might arise from the random motion of absorbers with respect to quasars.

Key words. Methods: statistical—quasars: general—quasars: absorption lines.

1. Introduction

Absorption lines are commonly detectable in quasar spectra. Material located along the line of sight of quasars at various distances would give rise to absorptions in the quasar spectra. Measurement of the absorption lines provides a useful tool to probe the invisible objects or gases, surrounding or inside galaxies. Absorption lines are traditionally split into two classes in terms of the relative velocity ($v_{\rm r}$) with respect to the quasar: (1) intervening absorption lines ($v_{\rm r} > 3000$ km s^{-1}, e.g., for the Mg II $\lambda\lambda 2796, 2803$ absorption doublet) and (2) associated absorption lines ($v_{\rm r} < 3000$ km s^{-1}).

The intervening absorption lines are often believed to be the absorptions caused by the cosmologically intervening foreground galaxies lying on the lines of sight of quasars (Bahcall & Spitzer 1969; Bergeron 1986; Bond *et al.* 2001; Chen & Tinker 2008; Bowen David & Chelouche 2011; Rogerson & Hall 2012). The strengths of the intervening absorption lines are believed to be related to the star formation rate (Guillemin & Bergeron 1997; Ménard *et al.* 2011) as well as the impact distance between the absorber and the central region of the corresponding galaxy (Chen *et al.* 2010).

The associated absorption lines are very important to reveal the physical conditions and dynamical mechanisms nearby or within the quasars, such as dust content, ionization state of gas, energetics and kinematics. The broad absorption lines imprinted in the quasar spectra, with line widths > 2000 km s^{-1} (Weymann *et al.* 1991), are undoubtedly associated with the quasars. The narrow absorption lines associated with the quasars, with line widths less than a few hundred km s^{-1} and often less than 100 km s^{-1}, are more common than the broad absorption lines (Richards 2001; Wild *et al.* 2008; Shen & Ménard 2012).

Outflows from quasars driven by the accretion process appear to be a natural event (Blandford & Payne 1982; Begelman 1985; Proga 2007), of which speeds range from a few hundred km s^{-1} (Crenshaw *et al.* 2000) to 10^4 km s^{-1} (Trump *et al.* 2006). They are detected most conspicuously via broad absorption lines in quasar spectra (Weymann *et al.* 1991). The outflows from quasars can also give rise to narrow absorption lines in their spectra (Nestor *et al.* 2008; Wild *et al.* 2008; Chen & Qin 2013; Chen *et al.* 2013a, b), which tend to correspond to the absorbers with $z_{\rm abs} \leq z_{\rm e}$. One of the possible reasons why broad absorption lines differ from narrow associated absorption lines is that outflows are observed at different orientations. Broad absorption lines might arise from the outflows with their directions being nearby the accretion disk planes, while narrow associated absorption lines might originate from the outflows with their directions being near to the spin axes of the accretion disks (see, e.g. Fig. 4 of Hamann *et al.* 2012).

It is widely accepted that the absorption line redshift is smaller than the corresponding emission line redshift of quasars, since only the foreground material with respect to the quasar can give rise to absorptions in the quasar spectra. However, for a small number of quasars some absorption line redshifts are greater than the corresponding emission line redshifts ($z_{\rm abs} > z_{\rm e}$) (Ryabinkov *et al.* 2003; Lü *et al.* 2007; Vanden Berk *et al.* 2008; Shen & Ménard 2012), which are undoubtedly associated to the quasars. Using 256 absorption systems with $z_{\rm abs} > z_{\rm e}$, Lü *et al.* (2007) firstly noticed a bimodal distribution for the Doppler redshifts ($z_{\rm Dopp}$, see the definition below). They ascribed the absorbers with larger $z_{\rm Dopp}$ to the material falling toward the central regions of quasars. However, up to now, no compelling evidence has ever showed that the infalling material originates from the returning gas of quasar jets or outflows, or from others.

Besides the outflows from quasars and the infalling material to the central region of quasars, the associated absorption lines can also arise from (1) the halos of quasar host galaxies (Crenshaw *et al.* 2004; Chelouche *et al.* 2008); (2) the vicinity of the black hole (Rees 1970; Barlow & Sargent 1997); (3) the external galaxies (Richards *et al.* 1999; Wild *et al.* 2008). The ionizing radiation comes from quasars, and therefore absorbers of the higher ionization associated absorption lines lie likely at smaller distances from the quasars (Barlow *et al.* 1997; Vanden Berk *et al.* 2008; Wild *et al.* 2008), and the optical thick absorbers around the quasars are likely anisotropic (Hennawi & Prochaska 2007), and therefore there would be an under-density of common absorption systems along the line-of-sight.

In this paper, we will utilize the sizeable and available Mg II associated absorber catalog of Sloan Digital Sky Survey (SDSS) quasar to investigate the distribution of Doppler redshift and their implication. This paper is organized as follows: In section 2, we describe the Mg II associated absorption systems. In section 3, we show the distribution of Doppler redshifts. The main analysis about the distribution of

Doppler redshifts are presented in section 4. We present the discussions in section 5 and a summary in section 6. Throughout this paper, we adopt the cosmology model with $\Omega_{\rm M} = 0.3,\ \Omega_\Lambda = 0.7$ and $H_0 = 70$ km s^{-1} Mpc^{-1}.

2. Data

The newest Mg II associated absorber catalog of SDSS quasar is that presented by Shen & Ménard (2012), which contains 1937 absorption systems (hereafter the SM12 sample) and becomes the most sizeable sample of this kind so far. The authors searched all the quasar spectra of SDSS DR7 (Schneider *et al.* 2010) with Mg II emission line coverage (about 85,000 quasars) for Mg IIλλ2796, 2803 associated absorption doublets. Adopting the method of Shen *et al.* (2011) and constraining within 2200–3090 Å in the quasar rest-frame, Shen & Ménard (2012) fitted a pseudo-continua with a power-law function plus a UV iron template provided by Vestergaard & Wilkes (2001), and fitted Mg II emission lines with multi-Gaussian functions. On both sides of the Mg II emission line, they identified Mg II λλ2796, 2803 absorption doublets from the spectrum that has subtracted the pseudo-continua and emission lines, and utilized a pair of Gaussian functions to measure the equivalent width of absorption lines. Only the absorption systems that were detected at $> 3\sigma$ for each Gaussian component and with $v_{\rm r} < 3000$ km s^{-1} (which were calculated with the emission redshifts based on the broad Mg II centroid) were selected.

3. Distribution of Doppler redshifts

Absorption line redshifts of quasars are the redshifts caused by cosmological distances and/or Doppler motions of absorbers. The Doppler redshift of an absorber relative to the quasar is defined as $z_{\rm Dopp} = (z_{\rm abs} - z_{\rm e})/(1 + z_{\rm e})$. If the absorption redshift $z_{\rm abs}$ is obviously less than the corresponding emission redshift $z_{\rm e}$, such as in the case of classical intervening absorption systems of quasars ($v_{\rm r} \gg 3000$ km s^{-1}, or $-z_{\rm Dopp} \ll 0.01$ for Mg II absorption lines), the difference between $z_{\rm abs}$ and $z_{\rm e}$ must mainly be due to the cosmological distance between the absorber and the quasar, where the contribution of the Doppler motion is relatively small. However, in the case of associated absorption lines, the value of $z_{\rm abs}$ is quite close to the corresponding $z_{\rm e}$ of the quasar. In this situation, the difference between $z_{\rm abs}$ and $z_{\rm e}$ would mainly be due to the Doppler motion of absorbers relative to the quasars (Kembhavi & Narlikar 1999).

In calculating the Doppler redshift, measurement of the quasar emission redshift is important. A systematic bias might alter the form of the Doppler redshift distribution. When one associated Mg II absorption system locates at the top of a Mg II broad emission line, the shape of the latter will be altered and then will affect its centroid. Compared to that determined from the narrow emission line, such as from [O III] emission lines, this might give rise to a different value of the emission redshift. Indeed, Vanden Berk *et al.* (2008) noted that the kinematic distribution with respect to the systematic quasar redshifts based on Mg II emission lines differs from that based on [O II] lines.

A catalog of improved redshifts for SDSS quasars was provided by Hewett & Wild (2010, hereafter HW), which were derived by cross correlating observed

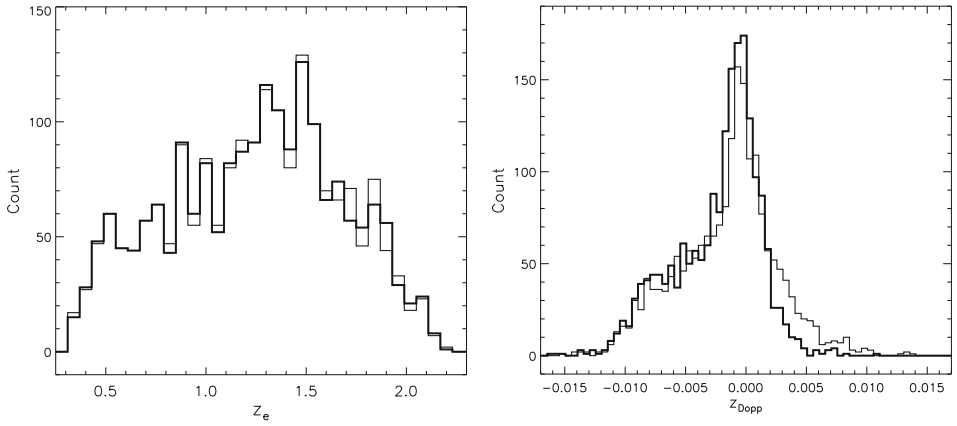

Figure 1. *Left panel*: the distributions of emission redshifts. *Right panel*: the distributions of Doppler redshifts. The thin solid line represents the data based on the SDSS emission redshifts, and the thick line stands for that based on the HW emission redshifts.

spectra with a carefully constructed template. In the left panel of Fig. 1, we show the distributions of the HW and SDSS emission redshifts of the quasars included by SM12 sample. Here, we do not find a significant difference for these two kinds of emission redshifts, based on the probability of the Kolmogorov–Smirnov (KS) test. We calculate Doppler redshifts of the SM12 sample, with the HW emission redshifts and the SDSS emission redshifts respectively. The distributions of the two kinds of Doppler redshift are shown in the right panel Fig. 1. However, it shows that Doppler redshifts calculated with the SDSS emission redshifts significantly differ from those calculated with the HW emission redshifts. The histogram of the latter Doppler redshifts exhibits a higher peak at $z_{\rm Dopp} \simeq 0.00$ and a lower wing on the positive $z_{\rm Dopp}$ side. For this sample of quasar absorbers, a KS-test shows that, the probability that the two distributions arise from the same population is $P < 10^{-9}$. In the following analysis, only the HW emission redshifts are adopted to calculate Doppler redshifts.

4. Analysis

4.1 *The highest peak of the distribution*

An asymmetric form of the Doppler redshift distribution is clearly seen in Fig. 1. However, it seems that a Gaussian function might be able to account for the highest peak of the distribution. We invoke a single Gaussian function to fit the distribution confined in the range of $z_{\rm Dopp} > -0.002$. We get $\sigma = 0.0014$, the central value of -0.0004, and the reduced $\chi^2 = 3.596$ for the fitting. The fitting result is shown in Fig. 2. The Gaussian component of the Doppler redshift distribution located at $z_{\rm Dopp} \simeq 0.00$ has already been noticed by Qin *et al.* (2004) and Lü *et al.* (2007). The Gaussian distribution of $z_{\rm Dopp}$ located at $z_{\rm Dopp} \simeq 0.00$ is expected if these absorbers are inside the same clusters of the quasars and their motions with respect to these quasars are random.

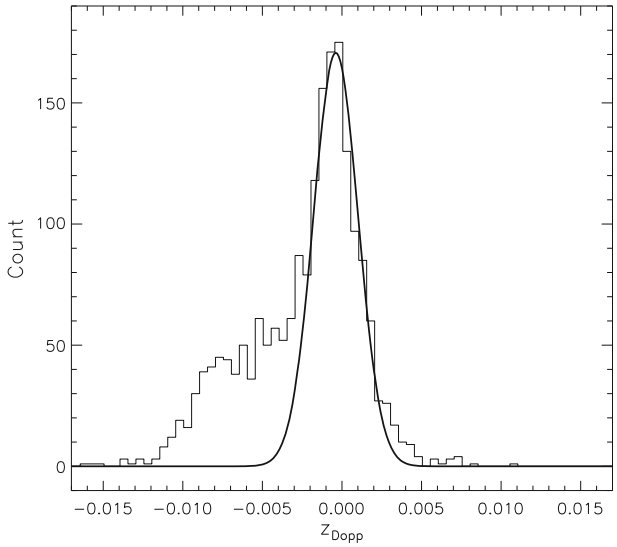

Figure 2. A single Gaussian fit (thick line) to the distribution (thin line) of Doppler redshifts of the SM12 sample, confined within the range of $z_{\rm Dopp} > -0.002$. The Doppler redshifts are calculated with the HW emission redshifts.

4.2 *The excess of $z_{\rm Dopp}$ in the positive region*

An obvious and a mild excess of $z_{\rm Dopp}$ are observed in the negative and positive regions, respectively compared with the single Gaussian fit shown in Fig. 2. The excess of $z_{\rm Dopp}$ in the positive values of $z_{\rm Dopp}$ was also observed by Lü *et al.* (2007), who showed a double-peaked structure for the distribution of Doppler redshifts, with one peak being located at $z_{\rm Dopp} \simeq 0.00$ and the other at $z_{\rm Dopp} \simeq 0.01$. In Fig. 2, the mentioned first peak is also shown, while the mentioned second peak is not obviously seen. In our sample, if the bimodal structure with one located in the positive Doppler redshift range exists as well, the position of the positive Doppler redshift peak must be less than 0.005 (see Fig. 2), significantly discrepant from the values obtained by Lü *et al.* (2007).

Lü *et al.* (2007) interpreted their positive Doppler redshift peak as the material falling towards the central region of quasars. The excess of Doppler redshifts with respect to the Gaussian distribution in the positive $z_{\rm Dopp}$ region might mainly or partially be caused by the infalling material, but its origin is unclear. The infalling material may (1) originate from the gas ejected from the quasar and then subsequently be overcome by gravitation (e.g., returning gas of jets or outflows) (Kippenhahn *et al.* 1974), (2) originate in the cloud within the host galaxy of the quasar that is accreted onto the central region of the quasar (Williams 1970). If that, the mild excess of $z_{\rm Dopp}$ in the positive region might suggest that there would be very little evidence for infalling gas towards the quasars.

Following the work of Lü *et al.* (2007), we employ a pair of Gaussian functions to fit the distribution of Doppler redshifts confined within $z_{\rm Dopp} > -0.002$, attempting to check if the excess of $z_{\rm Dopp}$ in the positive region can be accounted for by a

Gaussian function. The fitting yields $\sigma = 0.0027$ and the central value of -0.0001 for the first Gaussian function; $\sigma = 0.0013$ and the central value of -0.0005 for the second Gaussian function; and the reduced $\chi^2 = 1.146$ for the fitting. The result of the two Gaussian fit is plotted in Fig. 3. It shows that the fitting of a pair of Gaussian functions can match well the distribution of Doppler redshifts in the range of $z_{\rm Dopp} > -0.002$. The second peak of the distribution located at the positive Doppler redshift region shown in Lü *et al.* (2007) is not observed in our sample. Both Gaussian components in our fitting is located at $z_{\rm Dopp} \simeq 0.000$. All the absorption redshifts of SM12 are measured from the λ2796 line, therefore they are uniform. However, the absorption redshifts included in the sample of Lü *et al.* (2007) are not uniform: some determined by Lyman Limit Systems (LLSs); some by Damped Lyα systems (DALs); some by Broad Absorption Lines (BALs), etc (see Lü *et al.* 2007 for details). We note that the emission redshifts measured with different methods could give rise to a discrepancy of $z_{\rm Dopp}$. The event that the second peaked distribution of $z_{\rm Dopp}$ of Lü *et al.* (2007) does not appear in Fig. 2, probably originates from the absorption redshifts measured by different absorption lines.

The two Gaussian components shown in Fig. 3 are expected if the motions of these absorbers belong to two kinds of random motion. Perhaps absorbers of the narrow Doppler redshift distribution might locate at greater distances with respect to the central regions of the quasars while absorbers of the broad Doppler redshift distribution might be closer to the central regions. However, this interpretation is not favored by the analysis below, since to account for the positive excess, one has to have a better alternative.

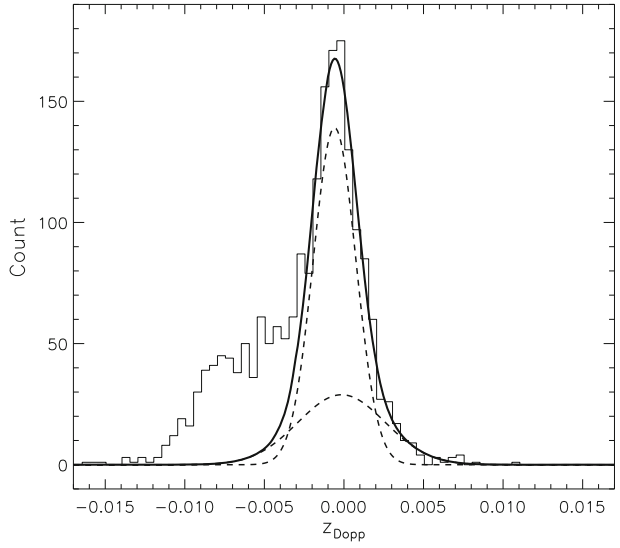

Figure 3. A two Gaussian fit to the distribution of Doppler redshifts (calculated with the HW emission redshifts) of the SM12 sample, confined within the range of $z_{\rm Dopp} > -0.002$. The dashed lines represent the two Gaussian components and the thick solid line stands for the fit which is just the sum of the two dashed lines.

4.3 *The excess of $z_{\rm Dopp}$ in the negative region*

As shown in Fig. 2, the excess of Doppler redshifts compared with a single Gaussian fit is much more significant in the negative $z_{\rm Dopp}$ region than that in the positive $z_{\rm Dopp}$ region. If the absorbers are inside the host galaxies (including their halos) of quasars, the negative $z_{\rm Dopp}$ likely implies that the absorbers systematically move away from the central region of the quasars. Outflows with high speeds giving rise to narrow absorption lines in quasar spectra seem to be very common (e.g., Nestor *et al.* 2008; Hamann *et al.* 2011). Therefore, the excess of $z_{\rm Dopp}$ in the negative region might arise from the outflows or jets of quasars.

The idea of accreting gas onto the supermassive black hole at the center of each galaxy as the energy source of active galactic nuclei is widely accepted. The primary optical and ultraviolet continuum emission is thought to arise from the thermal emission of geometrically thin and optically thick accretion disks (Shields 1978; Malkan 1983; Marconi *et al.* 2004). Emission from the accretion disks is anisotropy. The accretion disks emit more radiation along the directions of the corresponding spin axes (Laor & Netzer 1989; Sun & Malkan 1989; Kawaguchi & Mori 2010). Therefore, the observed optical and ultraviolet continuum emission from the accretion disk would strongly be associated with the inclinations between the lines of sight and the spin axes of accretion disks (Peterson 1997; Hubeny *et al.* 2000).

All of the quasar spectra analysed by Shen & Ménard (2012) have been analysed by Shen *et al.* (2011) as well. Using a power-law function plus a UV iron template provided by Vestergaard & Wilkes (2001), Shen *et al.* (2011) have fitted a pseudo-continua for each quasar spectrum of their sample. Depending on the emission redshift of quasars, they have also measured the pseudo-continua luminosity of quasars at rest-frame 1350 Å, 3000 Å or 5100 Å (directly measured from the pseudo-continua flux density at the corresponding wavelength). In this paper, we simply adopt the pseudo-continua luminosity of quasars at rest-frame 3000 Å from Table 1 of Shen *et al.* (2011) for our analysis. In Fig. 4 we show the distribution of continuum luminosities of quasars at rest-frame 3000 Å for the SM12 sample. We invoke a single Gaussian function to fit the distribution, which yields $\sigma = 0.4186$ and the central value of $\log L_{3000} = 45.61$ erg s^{-1}.

In order to check the effect of disk inclination on the distribution of $z_{\rm Dopp}$, we turn to consider the following two groups of quasars: (1) $\log L_{3000} \leq 45.61 - \sigma$ erg s^{-1} (we call the corresponding absorbers as sample A which includes 335 absorbers), here $\log L_{3000} = 45.61$ erg s^{-1} is the central value of the Gaussian fitting in Fig. 4 and $\sigma = 0.4186$ is its standard deviation; (2) $\log L_{3000} \geq 45.61 + \sigma$ erg s^{-1} (we call the corresponding absorbers as sample B, including 333 absorbers). The former sample might tend to correspond to the accretion disks of quasars with larger inclinations, while the latter sample might tend to be associated with that of smaller inclinations. In Fig. 5, we plot the distributions of $z_{\rm Dopp}$ for these two samples. It can be seen from Fig. 5 that $z_{\rm Dopp}$ distribution of sample A differs significantly from that of sample B. A Kolmogorov–Smirnov (KS) test shows that the probability of the two distributions arising from the same population is 1.93×10^{-10}. Generally speaking, when the directions of outflows or jets along the spin axes of accretion disks are close to the lines-of-sight, the more luminous continuum luminosities would be observed. It is reasonable that the smaller the inclinations between the spin axes of accretion disks and the lines-of-sight, the more and higher speed outflow materials

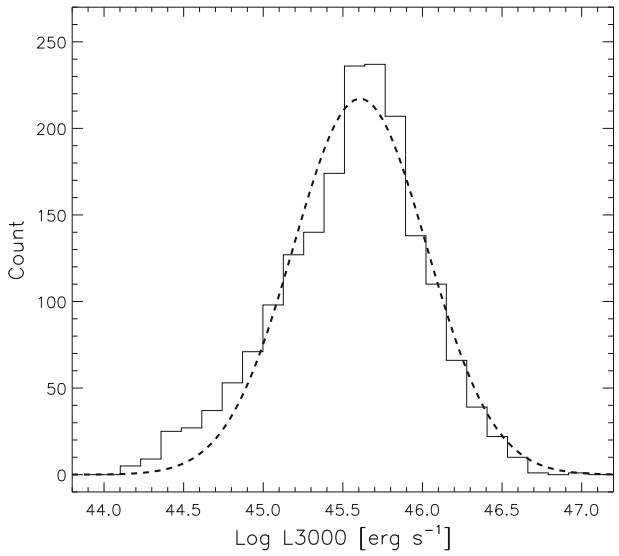

Figure 4. Distribution of continuum luminosities of quasars at rest-frame 3000 Å. The thick dashed line represents a single Gaussian fitting.

are observed. Assuming that absorbers of brighter quasars are associated with smaller accretion disk inclination angles and absorbers of fainter quasars are associated with larger accretion disk inclination angles, and some of the absorbers arise

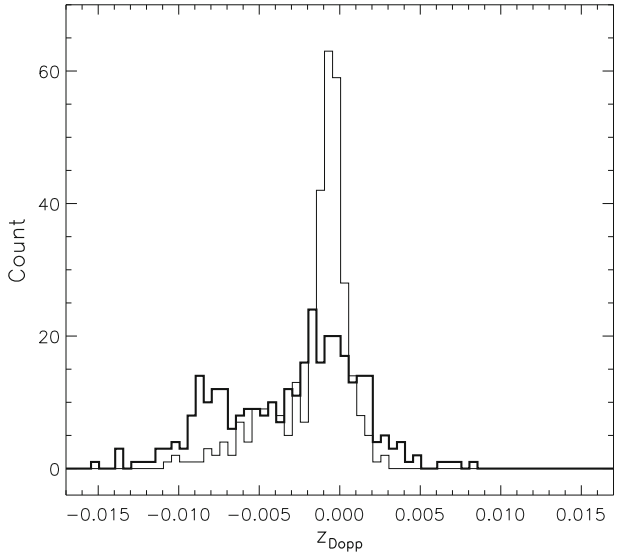

Figure 5. Distributions of Doppler redshifts of two sub-sets of absorbers. The thin histogram represents the absorbers of sample A, and the thick histogram represents the absorbers of sample B.

from the outflow materials, the excess of the $z_{\rm Dopp}$ distribution in the negative $z_{\rm Dopp}$ region of absorbers of brighter quasars is expected to be more obvious than that of fainter quasars (see the thick and thin histograms in Fig. 5).

A bimodal structure is clearly seen in the Doppler redshift distribution of sample B. We invoke a pair of Gaussian functions to fit the Doppler redshift distribution of sample B, which yields $\sigma = 0.0020$ and the central value of -0.0075 for the first Gaussian function; $\sigma = 0.0021$ and the central value of -0.0007 for the second Gaussian function; and the reduced $\chi^2 = 0.815$ for the fit. The fitting result is plotted in the right panel of Fig. 6 and presented in Table 1. A pair of Gaussian functions are also invoked to fit the Doppler redshift distribution of sample A, which yields $\sigma = 0.0037$ and the central value of -0.0027 for the first Gaussian function; $\sigma = 0.0008$ and the central value of -0.0005 for the second Gaussian function; and the reduced $\chi^2 = 1.029$ for the fitting. The fitting result is plotted in the left panel of Fig. 6 and also presented in Table 1.

It can be seen from Fig. 6 that a pair of Gaussian functions can well describe the Doppler redshift distributions of samples A and B. Meanwhile, the two Gaussian components shown in each panel correspond to different central values, with one centre being located at $z_{\rm Dopp} \simeq 0.000$ and the other centre at a position of a much smaller $z_{\rm Dopp}$ value. In each panel, the two Gaussian components probably have different origins. The Gaussian component located at $z_{\rm Dopp} \simeq 0.000$ might arise from common random motions of the absorbers with respect to the central regions of the quasars, and the other Gaussian component might arise from the absorbers with random motions as well but they possess a systematic outward motion with respect to the central regions of the quasars. Perhaps the latter absorbers belong to the set of material that have been driven from the central regions some time before (called absorbers with outflow histories) and therefore have a collective behavior later (e.g., to possess a collective speed of moving away from the corresponding

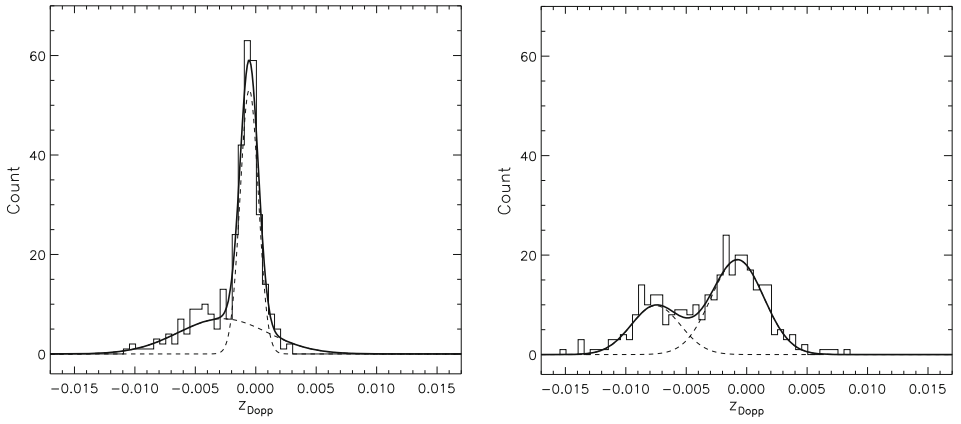

Figure 6. Fits of a pair of Gaussian functions to the Doppler redshift distributions of samples A (*left panel*) and B (*right panel*). For each panel, the dash lines represent the two Gaussian functions of the fit, and the thick solid line stands for the whole fitting curve which is just the sum of the two dashed lines.

Table 1. The fitting results of samples A and B.

	Gaussian central value	Dispersion (σ)	Gaussian central value	Dispersion (σ)	χ^2
Sample A	−0.0027	0.0037	−0.0005	0.0008	1.029
Sample B	−0.0075	0.0020	−0.0007	0.0021	0.815

central regions). We also noticed from Fig. 6 that the first central value of the Gaussian component of sample B (the absorber sample of brighter quasars), located at $z_{\rm Dopp} = -0.0075$, is obviously less than that of sample A (the absorber sample of fainter quasars), located at $z_{\rm Dopp} = -0.0027$. This might reflect the fact that absorbers with outflow histories have a larger collective speed in the direction of jets (where the quasars are generally brighter) than that in the direction far away from the jets (where the quasars are generally fainter).

Following Fig. 6, absorbers of our sample might have three origins, according to their motions and the inclinations of the accretion disk planes: (1) absorbers with outflow histories observed in the direction close to jets of quasars; (2) absorbers with outflow histories observed in the direction far away from jets of quasars; (3) absorbers with common random motions. These types of absorbers might form their own Doppler redshift distributions which are significantly distinct from each other. Based on this assumption, we consider the joining of three Gaussian functions to fit the distribution of $z_{\rm Dopp}$ of the SM12 sample, which yields $\sigma = 0.0021$ and the central value -0.0074 for the first Gaussian function; $\sigma = 0.0030$ and the central value -0.0017 for the second Gaussian function; $\sigma = 0.0012$ and the central value -0.0004 for the third Gaussian function; and the reduced $\chi^2 = 1.195$ for the fit. The fitting result is shown in Fig. 7 and presented in Table 2.

Perhaps the highest peak of the distribution could be accounted for by two Gaussian functions centered at $z_{\rm Dopp} = 0.0000$, just as that illustrated in Fig. 3. We employ a combination of four Gaussian functions to fit the distribution, assigning two of them located at $z_{\rm Dopp} = 0.0000$. The analysis produces a larger reduced χ^2 ($\chi^2_{\rm dof} = 1.509$), and the fit becomes worse (the details of the analysis are omitted). We therefore tend to believe that three Gaussian functions are enough to account for the Doppler redshift distribution of the SM12 sample. The previous interpretation of Fig. 3 is not favored, since to account for the excess of $z_{\rm Dopp}$ in the positive region, we have a better alternative (the second Gaussian function illustrated in Fig. 7).

4.4 *The Doppler redshift distributions vs. emission redshifts*

Here, we test whether there is an evidence for the redshift evolution in the Doppler redshift distributions. Therefore, we divide the SM12 into the lower emission redshift sample for $z_{\rm e} \leq 1.3103$ and the higher emission redshift sample for $z_{\rm e} > 1.3101$, where $z_{\rm e} = 1.3103$ is the median emission redshift of SM12. The Doppler redshift distributions of the two samples are shown in Fig. 8. A KS test to the two distributions yields a probability of $P < 10^{-5}$, which implies that they are significantly different from each other. Here, we also consider the joining of three Gaussian functions to fit the Doppler redshift distribution of the two samples. For the lower

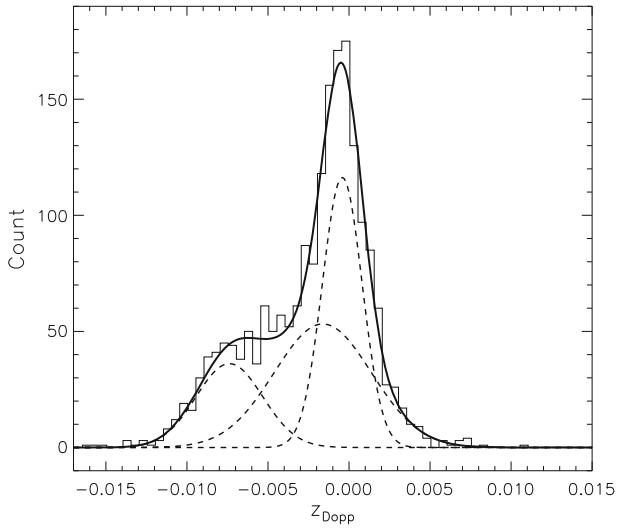

Figure 7. Three Gaussian fit to the distribution of Doppler redshifts of the SM12 sample, which are calculated with the HW emission redshifts. The thin dashed lines represent the three Gaussian fitting curves, and the thick solid line represents the whole fit which is just the sum of the three thin dashed lines. Area ratios of the fitting curves from left to right: 37.92%, 42.35%, and 19.71%.

emission redshift sample, the yields are $\sigma = 0.0022$ and the central value -0.0069 for the first Gaussian function; $\sigma = 0.0022$ and the central value -0.0011 for the second Gaussian function; $\sigma = 0.0008$ and the central value -0.0005 for the third Gaussian function; and the reduced $\chi^2 = 1.149$ for the fit. The fitting result is shown in the left panel of Fig. 9 and also presented in Table 2. And for the higher emission redshift sample, the yields are $\sigma = 0.0022$ and the central value -0.0069 for the first Gaussian function; $\sigma = 0.0022$ and the central value -0.0011 for the second Gaussian function; $\sigma = 0.0008$ and the central value -0.0005 for the third Gaussian function; and the reduced $\chi^2 = 0.970$ for the fit. The fitting result is shown in the right panel of Fig. 9 and presented in Table 2, as well.

4.5 *The Doppler redshift distributions vs. absorption strengths*

The distribution of absorption strengths is shown in the left panel of Fig. 10. The question is: does the absorption strength put a role on the Doppler redshift distributions? In order to test whether there are systematic differences between the Doppler redshift distributions of strong and weak MgII absorbers, here, we divide the SM12

Table 2. The fitting results of the joining of three Gaussian functions.

	Central value	σ	Central value	σ	Central value	σ	χ^2
Total sample	−0.0074	0.0021	−0.0017	0.0030	−0.0004	0.0012	1.195
Lower redshift sample	−0.0069	0.0022	−0.0011	0.0022	−0.0005	0.0008	1.149
Higher redshift sample	−0.0075	0.0021	−0.0018	0.0034	−0.0004	0.0019	0.970

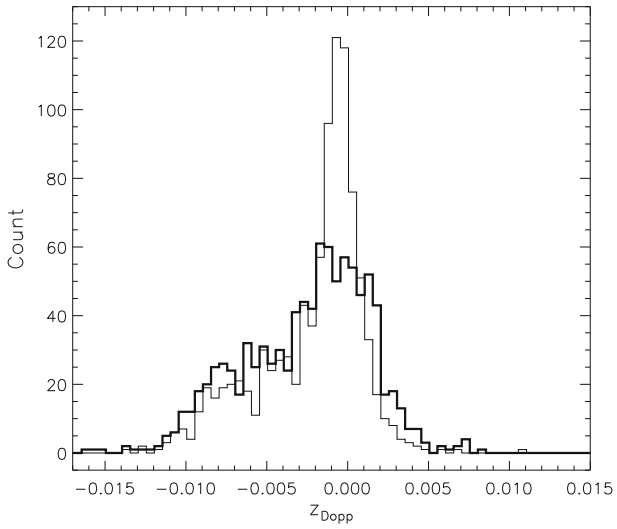

Figure 8. The Doppler redshift distributions for different emission redshifts. The thin solid line represents the absorption systems with $z_e \leq 1.3103$, and the thick solid line represents those with $z_e > 1.3103$.

into two subsamples based on the median absorption strength of λ2796 lines. That is the weak absorption sample with $W_r\lambda2796 \leq 1.22$Å and the strong absorption sample with $W_r\lambda2796$ 1.22Å, here $W_r\lambda2796 = 1.22$Å is the median absorption strength of λ2796 lines. The Doppler redshift distributions of the two samples are shown in the right panel of Fig. 10. For these samples of absorbers, a KS-test derives a value of $P > 12\%$. This manifests that the null hypothesis, that the two sub-samples arise

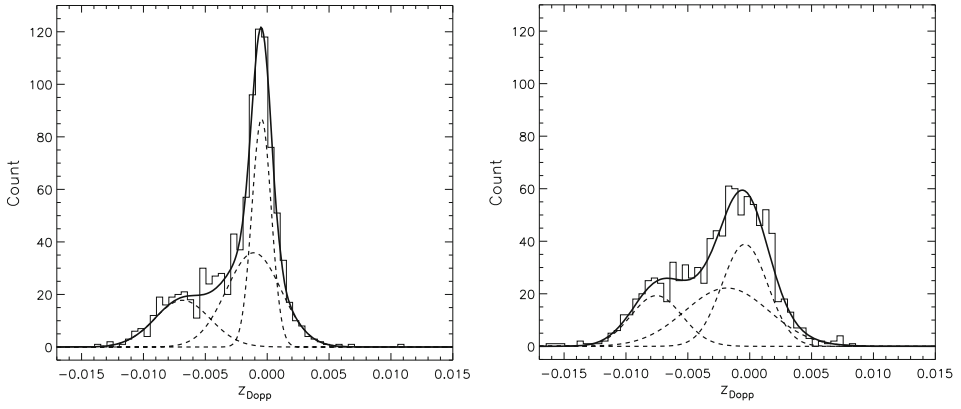

Figure 9. Fits of a joining of three Gaussian functions to the Doppler redshift distributions of the absorption systems with $z_e \leq 1.3103$ (*left panel*) and $z_e > 1.3103$ (*right panel*). For each panel, the dashed lines represent the three Gaussian functions of the fit, and the thick solid line stands for the whole fitting curve which is just the sum of the three dashed lines.

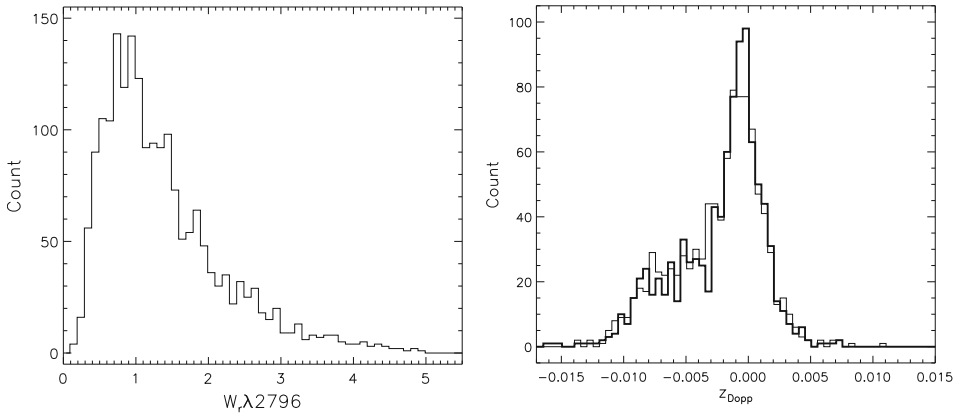

Figure 10. *Left panel*: the distribution of absorption strengths. *Right panel*: the Doppler redshift distributions for different strengths of λ2796 lines; the thin solid line represents the absorption systems with $W_r\lambda2796 \leq 1.22$Å, and the thick solid line represents the those with $W_r\lambda2796 > 1.22$Å.

from the same population, cannot be ruled out. Therefore, the absorption strength might contribute to the Doppler redshift distribution.

5. Discussions

One possible origination of the excess of $z_{\rm Dopp}$ in the negative region is from the contamination of intervening absorption systems. In other words, some of the absorption systems of the SM12 sample, with negative values of $z_{\rm Dopp}$, might in fact be Mg II intervening absorption systems, e.g., when the absorbers are quite close to the quasars. The intervening absorption of close absorbers cannot be picked out from the SM12 sample, and therefore this effect cannot be considered in this paper. However, as shown in Fig. 6, two Gaussian component fits can well describe the $z_{\rm Dopp}$ distributions of a brighter quasar sample (sample B) as well as a fainter quasar sample (sample A). This indicates that if there does exist the contamination of intervening absorption systems, the effect must be relatively mild for the sample concerned.

As discussed above, absorbers of quasars with different continuum luminosities correspond to different distributions of Doppler redshifts (see Fig. 5), which is interpreted as being due to different accretion disk inclination angles. Here, we try to check if absorbers with entirely different Doppler redshifts correspond to significantly different kinds of source. We select those quasars of the SM12 sample with only one detected Mg II associated absorption system and divide the corresponding absorbers into two groups according to the following conditions: (1) $z_{\rm Dopp} > -0.0004 - \sigma_3$ (sample C, including 970 quasars), here $z_{\rm Dopp} = -0.0004$ is the central value of the third Gaussian component in Fig. 7 and $\sigma_3 = 0.0012$ is its standard deviation; (2) $z_{\rm Dopp} < -0.0074 + \sigma_1$ (sample D, including 348 quasars), here $z_{\rm Dopp} = -0.0074$ is the central value of the first Gaussian component in Fig. 7 and $\sigma_1 = 0.0021$ is its standard deviation. The distributions of continuum luminosities of quasars of samples C and D, respectively, are shown in Fig. 11. A KS test

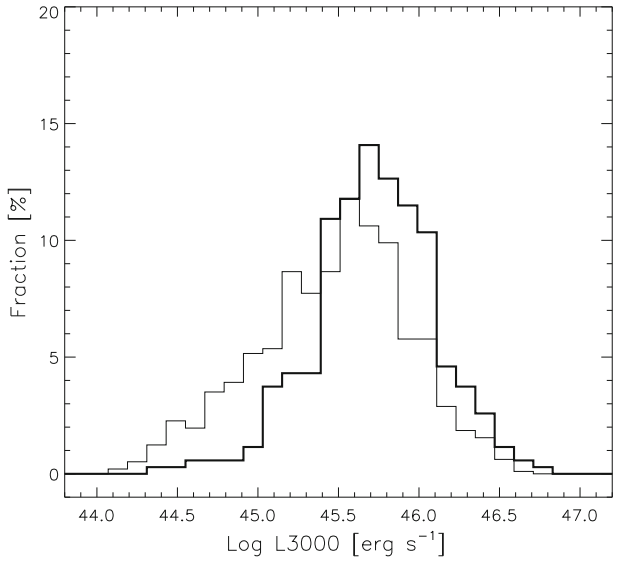

Figure 11. Distribution of continuum luminosities of quasars at rest-frame 3000 Å. The thin line histogram represents the continuum luminosities of quasars of sample C, and the thick line histogram describes the continuum luminosities of quasars of sample D.

shows that the probability that the continuum luminosities of quasars of the two samples arise from the same distribution is 2.99×10^{-14}. It implies that different ranges of Doppler redshifts do correspond to different continuum luminosities of quasars. Quasars of sample C are generally fainter than those of sample D. This must be due to the fact that, when the directions of jets are close to the lines-of-sight, quasars would tend to be more luminous and the speeds of the corresponding absorbers would tend to be larger. Therefore, the origin of the third Gaussian component (the one with its peak being located at $z_{\rm Dopp} = -0.0004$) in Fig. 7 differs from that of the first component (the one with its peak being located at $z_{\rm Dopp} = -0.0074$).

Does the completeness of the SM12 sample play an important role in forming the shape of its Doppler redshift distribution? Currently, the completeness of the sample is not well determined. Shen & Ménard (2012) mentioned that quantifying the completeness of their sample (the SM12 sample) requires a more dedicated narrow absorption finder. It is beyond the scope of this paper to find out the incompleteness of this sample, and therefore we are unable to discuss the incompleteness effect currently.

Suppose that there does exit a bias of the SM12 sample. Examining our analysis above, we do not find any bias that can give rise to the results shown in Figures 5 and 11. In fact, what is shown in Figures 5 and 11 are in agreement with the argument that, when the directions of jets are close to the lines-of-sight, quasars would tend to be more luminous and the speeds of the corresponding absorbers would tend to be larger. The main analysis of this paper is illustrated in Fig. 7, which is in good agreement with the argument. Although the incompleteness of the sample is unclear, it is unlikely that a bias of the sample can lead to an entirely different result. We therefore believe that, to some extent, what we have learned above in Fig. 7 might be true.

6. Summary

Using 1937 Mg II associated absorbers of SDSS DR7 identified by Shen & Ménard (2012), we have presented an analysis of their Doppler redshift distributions without accounting for the contamination of intervening absorption systems, which can not be picked out from our sample. Our analysis shows that there might exist three Gaussian components in the Doppler redshift distribution, with the first Gaussian component being located at $z_{\rm Dopp} = -0.0074$, the second Gaussian component at $z_{\rm Dopp} = -0.0017$, and the third Gaussian component at $z_{\rm Dopp} = -0.0004$. Our analysis shows that the three Gaussian components are likely to correspond to three origins, according to the motions of absorbers and the inclinations of the accretion disk planes. The first Gaussian component probably arises from absorbers with outflow histories observed in the direction close to jets of quasars. The second Gaussian component possibly arises from absorbers with outflow histories observed in the direction far away from jets of quasars. Whereas, the third Gaussian component might also arise from absorbers with random motion of absorbers with respect to quasars.

Acknowledgements

The authors would like to thank the anonymous referee for helpful comments and suggestions. This work was supported by the National Natural Science Foundation of China (No. 11363001, No. 11073007), the Guangxi Natural Science Foundation (2012jjAA10090), the Guangzhou Technological Project (No.11C62010685), and the Guangxi University of Science and Technology research projects (No. 2013LX155).

References

Bahcall, J. N., Spitzer, L. Jr. 1969, *ApJ*, **156**, L63.
Barlow, T. A., Hamann, F., Sargent, W. L. W. 1997, *ASPC*, **128**, 13.
Barlow, T. A., Sargent, W. L. W. 1997, *AJ*, **113**, 136.
Begelman, M. C. 1985, *ApJ*, **297**, 492.
Bergeron, J. 1986, *A&A*, **155**, L8.
Blandford, R. D., Payne, D. G. 1982, *MNRAS*, **199**, 883.
Bond, N. A., Churchill, C. W., Charlton, J. C., Vogt, S. S. 2001, *ApJ*, **562**, 641.
Bowen David, V., Chelouche, D. 2011, *ApJ*, **727**, 47.
Chelouche, D., Ménard, B., Bowen, D. V., Gnat, O. 2008, *ApJ*, **683**, 55.
Chen, H. W., Helsby, J. E., Gauthier, J. R. *et al.* 2010, *ApJ*, **714**, 1521.
Chen, H. W., Tinker, J. L. 2008, *ApJ*, **687**, 745.
Chen, Z. F., Li, M. S., Huang, W. R., Pan, C. J., Li, Y. B. 2013a, *MNRAS*, **434**, 3275.
Chen, Z. F., Qin, Y. P. 2013, *ApJ*, **776**, 1.
Chen, Z. F., Qin, Y. P., Gu, M. F. 2013b, *ApJ*, **770**, 59.
Crenshaw, D. M. *et al.* 2000, *AJ*, **120**, 1731.
Crenshaw, D. M., Kraemer, S. B., Gabel J. R. *et al.* 2004, *ApJ*, **612**, 152.
Guillemin, P., Bergeron, J. 1997, *A&A*, **328**, 499.
Hamann, F., Kanekar, N., Prochaska, J. X., *et al.* 2011, *MNRAS*, **410**, 1957.
Hamann, F., Simon, L., Hidalgo, P. R., Capellupo, D. 2012, arXiv:1204.3791.
Hennawi, J. F., Prochaska, J. X. 2007, *ApJ*, **655**, 735.
Hewett, P. C., Wild, V. 2010, *MNRAS*, **405**, 2302.
Hubeny, I., Agol, E., Blaes, O., Krolik, J. H. 2000, *ApJ*, **533**, 710.

Kawaguchi, T., Mori, M. 2010, *ApJ*, **724**, L183.
Kembhavi, A. K., Narlikar, J. V. 1999, *Quasars and Active Galactic Nuclei: An Introduction* (Cambridge: Cambridge Univ. Press).
Kippenhahn, R., Perry, J. J., Röser, H. J. 1974, *A&A*, **34**, 211.
Laor, A., Netzer, H. 1989, *MNRAS*, **238**, 897.
Lü, L. Z., Qin, Y. P., Cupta, A. C. 2007, *ApJ*, **669**, 74.
Malkan, M. 1983, *ApJ*, **268**, 582.
Marconi, A., Risaliti, G., Gilli, R. *et al.* 2004, *MNRAS*, **351**, 169.
Ménard, B., Wild, V., Nestor, D. *et al.* 2011, *MNRAS*, **417**, 801.
Nestor, D., Hamann, F., Rodriguez Hidalgo, P. 2008, *MNRAS*, **386**, 2055.
Peterson, B. M. 1997, *An Introduction to Active Galactic Nuclei* (Cambridge: Cambridge Univ. Press).
Proga, D. 2007, *ApJ*, **661**, 693.
Qin, Y. P., Liu, H. T., Liang, E. W. *et al.* 2004, *MNRAS*, **351**, 1319.
Rees, M. J. 1970, *ApJ*, **160**, L29.
Richards, G. T. 2001, *ApJS*, **133**, 53.
Richards, G. T., York, D. G., Yanny, B. *et al.* 1999, *ApJ*, **513**, 576.
Rogerson, J. A., Hall, P. B. 2012, *MNRAS*, **421**, 971.
Ryabinkov, A. I., Kaminker, A. D., Varshalovich, D. A. 2003, *A&A*, **412**, 707.
Schneider, D. P. *et al.* 2010, *AJ*, **139**, 2360.
Shen, Y., Ménard, B. 2012, *ApJ*, **748**, 131 (SM12).
Shen, Y., Richards, G. T., Strauss, M. A. *et al.* 2011, *ApJS*, **194**, 45.
Shields, G. A. 1978, *Nature*, **272**, 706.
Sun, W. H., Malkan, M. A. 1989, *ApJ*, **346**, 68.
Trump, J. R. *et al.* 2006, *ApJS*, **165**, 1.
Vanden Berk, D. E., Khare, P., York, D. G. *et al.* 2008, *ApJ*, **679**, 239.
Vestergaard, M., Wilkes, B. J. 2001, *ApJS*, **134**, 1.
Weymann, R. J., Morris, S. L., Foltz, C. B., Hewett, P. C. 1991, *ApJ*, **373**, 23.
Wild, V., Kauffmann, G., White, S., *et al.* 2008, *MNRAS*, **388**, 227.
Williams, R. E. 1970, *Nature*, **228**, 269.
York, D. G. *et al.* 2005, in *IAU Colloq. 199, Probing Galaxies through Quasar Absorption Lines* (Cambridge: Cambridge Univ. Press), 58.
York, D. G. *et al.* 2006, *MNRAS*, **367**, 945.